AN EMPIRICAL METHODOLOGY FOR THE DESIGN OF VERTICAL-TUBE ABSORBERS

Vikas Patnaik, Ph.D.
Student Member ASHRAE

William A. Miller, P.E.
Associate Member ASHRAE

Horacio Perez-Blanco, Ph.D.
Member ASHRAE

ABSTRACT

An analytical model was developed for the lithium bromide-water ($LiBr-H_2O$) vertical-tube absorber by Patnaik et al. (1993). Model output has been compared to experimental data from two different sources for the smooth tube: Jianpin et al. (1985) and Miller et al. (1992). The data gathered by the latter also include advanced absorber surfaces: pin-finned (three), grooved, fluted, and twisted tubes. The experimental comparisons were performed by running the model at the same operating conditions as those during which the experimental data were collected. The performances of all seven advanced tubes were predicted adequately (within ±20% overall) within the experimental ranges covered by the tests carried out by Miller. Finally, the model was used to generate design charts for each type of absorber tube. Examples of the charts are presented with guidelines for their use in the design of prototypes.

INTRODUCTION

After the development of an analytical model for a vertical-tube absorber (Patnaik et al. 1993) and before the translation of its results into an effective design methodology, it is necessary to verify the model. This verification involves the comparison of predicted absorber performance to experimental data obtained for a vertical-tube absorber under conditions identical to those input to the model.

The analytical model was originally developed for the smooth tube, for which various empirical and semi-empirical correlations on the heat and mass transfer coefficients exist in the literature (Patnaik et al. 1993). From the smooth-tube geometry, the model was extended to six additional absorber tube surfaces, represented in Figure 1 (the photograph of the pin-finned tube was taken before the fins were shaved to a height of 1/8 in.). The three pin-finned tubes and the grooved, fluted, and twisted tubes were simulated by modifying the model to accept empirical information in the form of heat and mass transfer coefficients for these surfaces. The modifications were based on suitable assumptions regarding the solution interface temperature. The model proved quite robust in terms of generality in that the performances of all six advanced tubes were reproduced adequately (within ±20% overall) within the experimental ranges covered by the tests carried out by Miller et al. (1992).

During model verification for the smooth tube, the presence of waves was encountered in the vertical falling film over the absorber tube. There are primarily two types of waves in falling films (Patnaik 1994)—high-frequency, small-amplitude, capillary waves (Levich 1962) and low-frequency, large-amplitude, inertial "roll" waves (Brauner 1989). The former type occurs in the flow range of $20 < Re_s < 200$, while the film surface is characterized by the latter type for $Re_s > 200$. The waves are known to originate due to hydrodynamic instability in the film but can also be induced mechanically or by the addition of surfactants. Capillary waves can cause 30% more absorption than that predicted by smooth-film theory (Ruckenstein and Berbente 1968). Roll waves, on the other hand, have been shown to cause an enhancement of as much as 250% (Wasden and Dukler 1990) by periodically convecting species (and energy) in the transverse and then streamwise directions (Patnaik 1994). Through image-processing studies (Patnaik 1994), the waves detected on Miller's absorber tube were established to be roll waves.

SMOOTH-TUBE COMPARISONS

The first data source employed for model verification was that of Jianpin et al. (1985). Excellent agreement between experimental data and model output was obtained for the five runs reported (within 10% for mass absorbed and less than 0.5% for heat load), at an absorber pressure of 6.4 mm Hg. The extent of the agreement is shown in Figures 2 and 3. Difficulties in experimental measurement could explain the discrepancy between the two agreements since an overall energy balance checks the consistency of the model results. The falling-film Reynolds number ranged approximately from 20 to 30 in these runs. At such low Reynolds numbers (Re), nearly laminar flow can be expected apart from the presence of capillary waves. The moderate mass transfer enhancement due to such waves is well accounted for in correlations by Yih and Chen (1982).

When the model was run for the experimental conditions set by Miller, underprediction by factors of as much as

Vikas Patnaik is a research engineer at Phillips Engineering Company, St. Joseph, MI. **Horacio Perez-Blanco** is an associate professor at Pennsylvania State University, University Park. **William A. Miller** is on the research staff at Oak Ridge National Laboratory, Oak Ridge, TN.

PIN-FINNED SURFACE: Tubes -1,-2,-3

* Spines shaved to 1/8 inch high for testing

- INTEGRAL FINS CUT FROM THE TUBING WALL ITSELF
- GEOMETRY: 26 FINS PER TURN
  5/8 INCH SPINE HEIGHT*
  1/4 INCH, 3/16 INCH, 1/8 INCH — SPINE PITCH
  0.840 INCH O.D. (UNDEFORMED)
  0.109 INCH WALL
- MATERIAL: 304L STAINLESS STEEL

TWISTED SURFACE: Tube-6

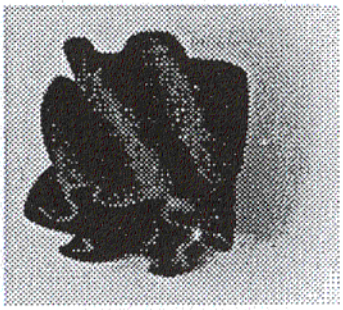

- TWISTING (STARTS) FORMED THROUGH EXTRUSION PROCESS
- GEOMETRY: 4 STARTS PER TURN
  45° HELIX ANGLE
  0.875 INCH O.D. (UNDEFORMED)
  0.026 INCH WALL
- MATERIAL: CARBON STEEL

FLUTED SURFACE: Tube-5

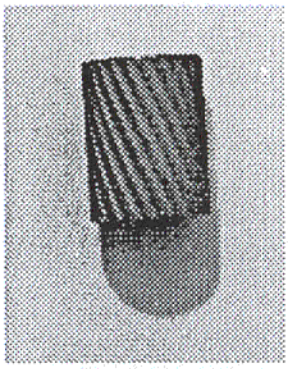

- FLUTES (STARTS) FORMED BY NUMERICALLY CONTROLLED MILLING MACHINE
- GEOMETRY: 24 STARTS PER TURN
  22° HELIX ANGLE
  0.025 INCH FLUTE DEPTH
  0.75 INCH O.D. (UNDEFORMED)
  0.095 INCH WALL
- MATERIAL: 304L STAINLESS STEEL

GROOVED SURFACE: Tube-4

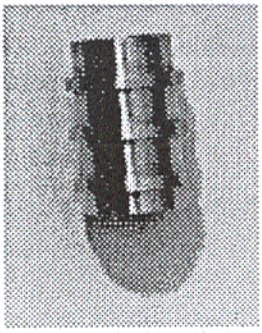

- GROOVES FORMED BY LATHE
- GEOMETRY: 0.75 INCH O.D. (UNDEFORMED)
  0.25 INCH PITCH
  0.06 INCH KNURL HEIGHT
- MATERIAL: 304 L STAINLESS STEEL
- DESIGN GLEANED FROM WORK OF DAVIES, J.T. AND WARNER, K.V.

Figure 1 *Advanced surfaces selected for testing.*

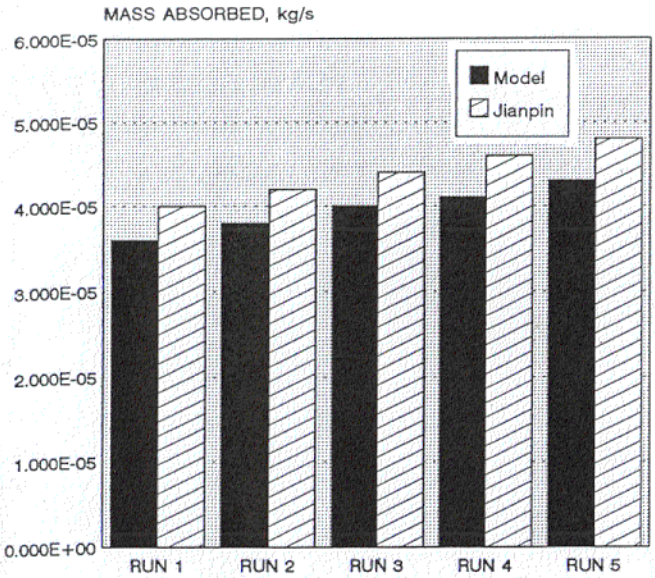

Figure 2 *Comparison with the data of Jianpin et al. (1985): mass absorbed.*

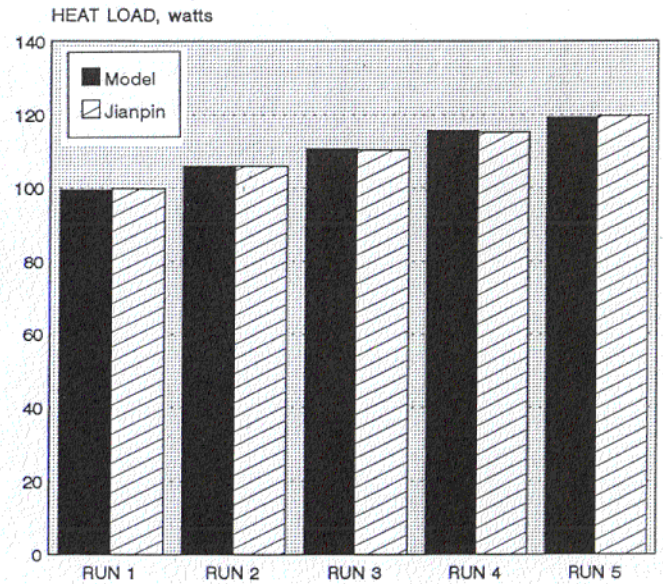

Figure 3 *Comparison with the data of Jianpin et al. (1985): heat load.*

3 to 4 was observed in the mass absorbed and the heat load. Reasons for the underprediction of experimental data were sought, and it appeared that the waves were enhancing mass transfer considerably. The effect of capillary waves was included as before, but the model had no information on the larger and faster roll waves observed in Miller's experimental setup.

To account for the roll waves, the model was modified as follows. First, an estimate of the average pressure differential between the absorber vapor pressure and the solution equilibrium pressure was obtained:

$$\Delta P = P_{v,absorber} - \frac{P_{s_i} + P_{s_{flash}} + P_{s_o}}{3}, \qquad (1)$$

where the possible effect of "flashing" at the solution inlet is included by calculating $P_{s_{flash}}$ as the solution pressure immediately downstream of the inlet restriction posed by the distributor cup (Miller et al. 1992). This "driving force" is related to the amount of mass absorbed by

$$\Delta m = \kappa_P A \Delta P, \qquad (2)$$

where κ_P is the pressure-based mass transfer coefficient. The presence of roll waves can thus be accounted for by an increase in κ_P or ΔP. Now, κ_P should simply be a function of flow and fluid properties. Since mass transfer *enhancement* was found to be related to absorber operating pressure, increasing κ_P would render it pressure-dependent, thereby reducing its usefulness and forcing, in cases of varying absorber pressure, iterative calculations. The ΔP driving force was more amenable to correction. This also prevented the possibility of numerical instabilities arising from large values of κ_P.

As shown in the pressure-correction map of Figure 4, at lower absorber pressures (i.e., when the solution is near vapor-pressure equilibrium), the driving force due to the roll waves is comparable to that due to the (actual) ΔP. With progressively increasing operating pressures, this effect (and hence the pressure correction) diminishes, and by about $P_{v,absorber}$ = 28 mm Hg, the ΔP almost solely provides the driving force for absorption.

The enhancement factors corresponding to the "effective" absorber pressures from Figure 4 were found to agree with those computed by Wasden and Dukler (Figure 7), defined with respect to mass transfer in waveless films as predicted by Higbie (Seban 1978). This comparison is shown in Figure 8, with the similarity of the enhancement factors being remarkable.

The experimental runs were screened for inconsistencies. Runs with negative or negligible pressure differential, as well as those with negative heat transfer coefficients, were excluded from the comparisons. For the remaining 55 runs, a roughly normal distribution emerged for both the mass absorbed and the heat load, with the mean of deviation from perfect agreement being –7.2% (Figure 5) and –20.6% (Figure 6), respectively. (Refer to Table 1 for complete statistics.) Thus, the underprediction is slightly greater in the case of the heat load. However, the sharp peak in the case of either distribution reflects the consistency in the comparisons.

MODEL FOR ADVANCED SURFACES

The model was also adapted to calculate Miller's advanced tube performance data. The experimental mass

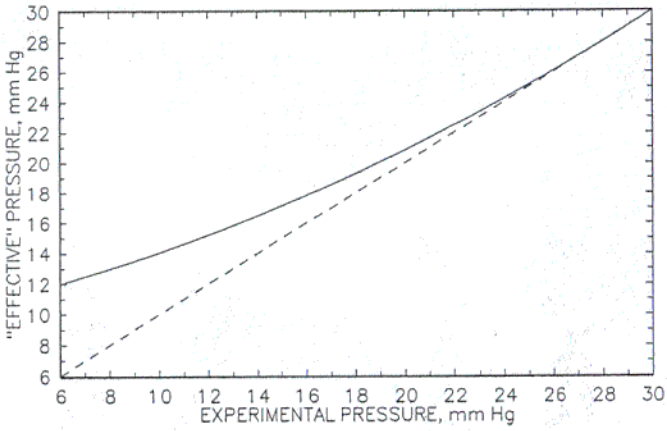

Figure 4 *Pressure correction map.*

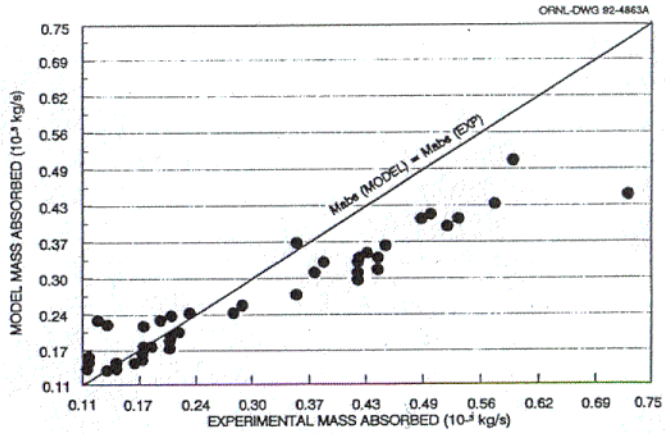

Figure 5 *Validation of mass absorbed for smooth tube. The effective pressure (Figure 4), accounting for roll waves, was used in the validation.*

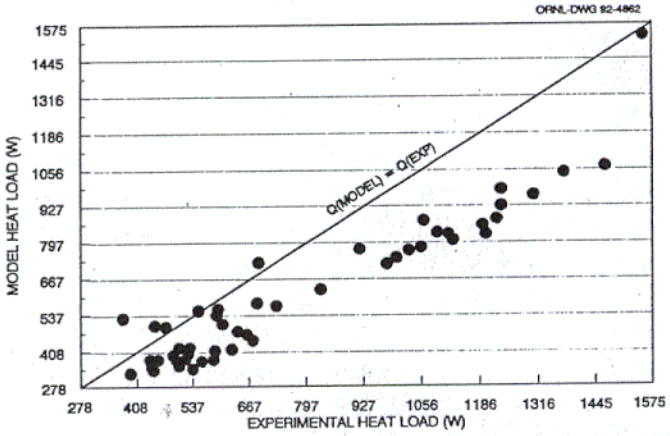

Figure 6 *Validation of heat load for smooth tube. The effective pressure (Figure 4), accounting for roll waves, was used in the validation.*

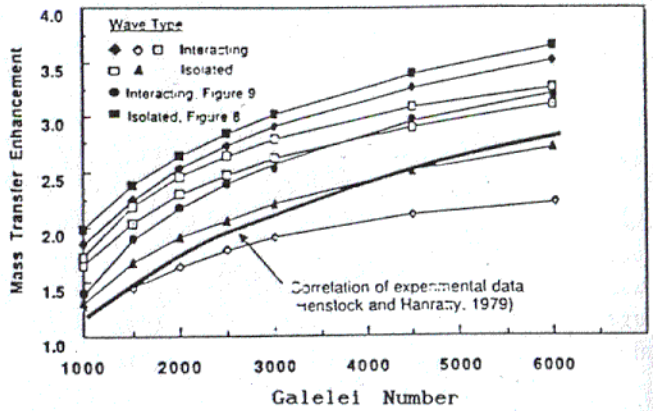

Figure 7 *Results of numerical model for roll waves (Wasden and Dukler 1990).*

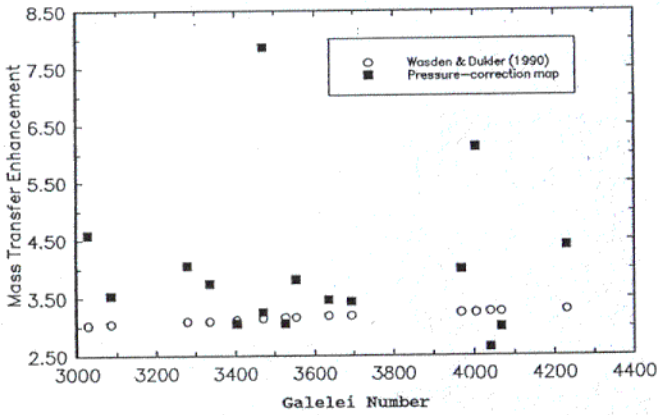

Figure 8 *Comparison of enhancement ratios.*

transfer coefficient was recalculated employing the following log-mean concentration difference approach:

$$\kappa = \frac{\Delta m''}{\mathrm{LMCD}}, \tag{3}$$

where

$\Delta m''$ = mass flux (kg/s·m^2), determined experimentally; and

$$\mathrm{LMCD} = \frac{[c_{s_i} - c(T_{s_i}, P_v)] - [c_{s_o} - c(T_{s_o}, P_v)]}{\ln\left[\dfrac{c_{s_i} - c(T_{s_i}, P_v)}{c_{s_o} - c(T_{s_o}, P_v)}\right]}. \tag{4}$$

For the overall heat transfer coefficient, no recalculation was required, and the experimental values were used by the model. The model recreated the experimental results as shown in Figures 9 and 10 and summarized in Table 1. The

ORNL-DWG 92-4864B

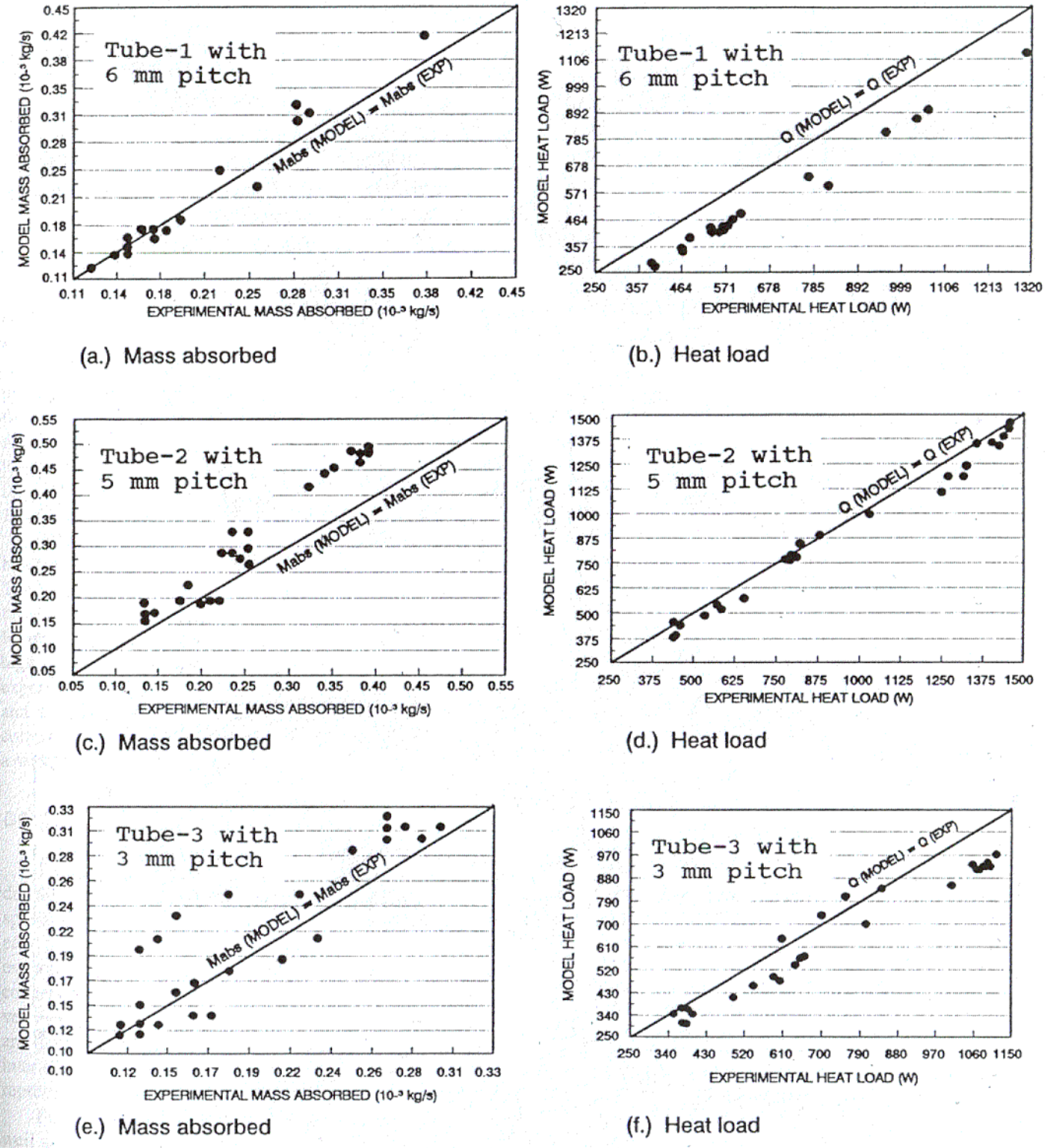

Figure 9 *Validation for pin-finned tubes having a spine height of 3 mm with 26 spines per turn.*

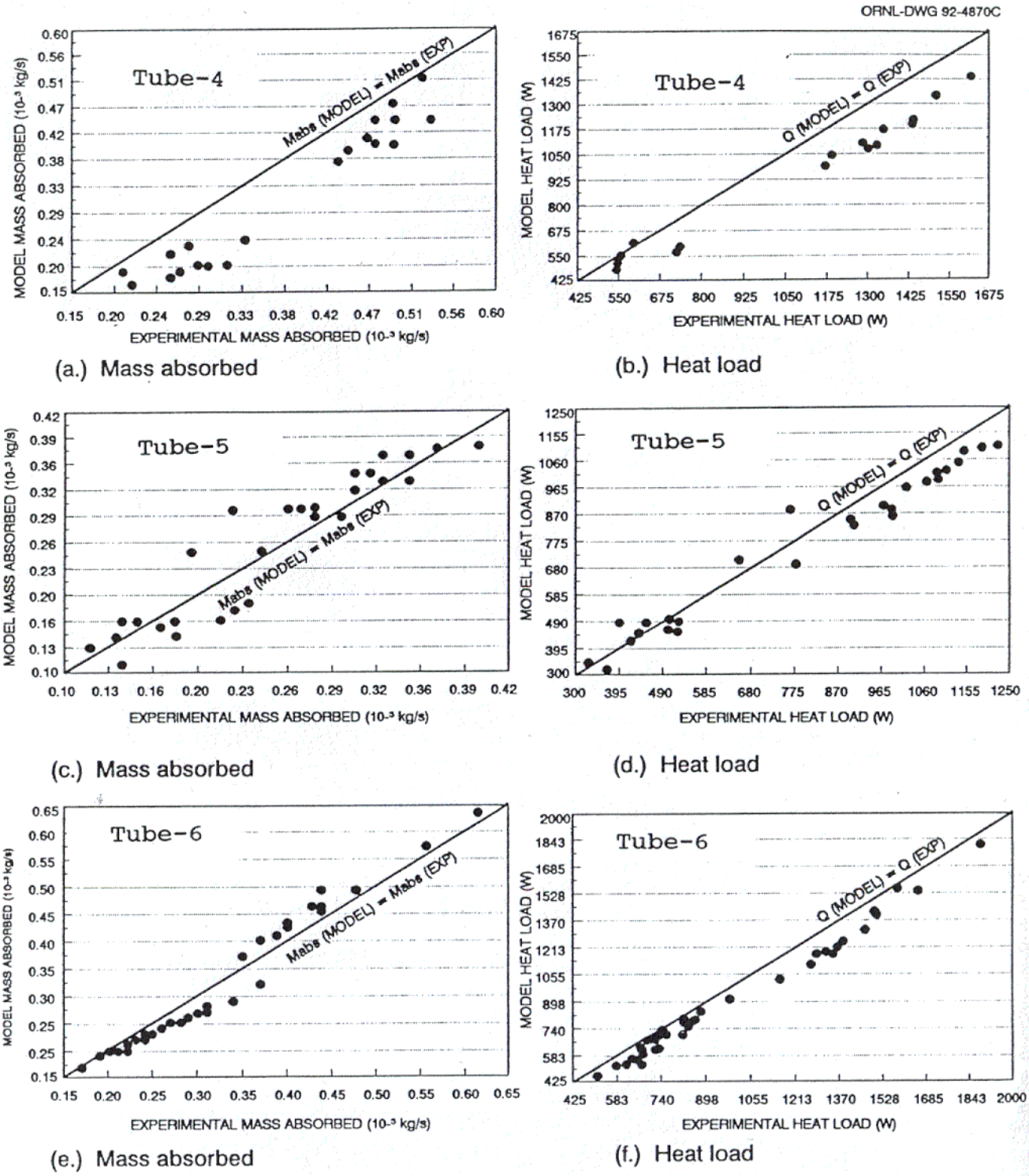

Figure 10 *Validation for grooved, fluted, and twisted tubes.*

TABLE 1
Parameters of Error Distribution as Percentage of Experimental Data: Mean and Standard Deviation of the Distribution

Tube Type	Mass Absorbed		Heat Load	
	Mean	Standard Deviation	Mean	Standard Deviation
Smooth (Roll Waves)	−7.2	19.4	−20.6	12.5
Tube −1	0.7	6.8	−17.9	2.7
Tube −2	16.6	11.2	−3.4	4.7
Tube −3	9.9	18.7	−9.3	8.0
Tube −4	−16.7	9.6	−9.5	7.4
Tube −5	1.1	14.2	−3.1	8.2
Tube −6	−2.8	7.1	−9.2	4.1

same considerations as for the smooth tube applied to the selection of the runs.

Good agreement was obtained between the model predictions and experimental data (the mean of deviation from perfect agreement was within ±17%) for mass absorbed (Figures 9a, 9c, 9e, 10a, 10c, and 10e). For the heat load, underprediction was observed, on average within 21%, for the advanced surfaces (Figures 9b, 9d, 9f, 10b, 10d, and 10f).

For tubes −4, −5, and −6, few runs yielded mass transfer coefficients that were in excess of 3×10^{-3} m/s. These were obtained for operating conditions similar to those that yielded coefficients more akin to Henstock and Hanratty's measurements (Wasden and Dukler 1990). Such high mass transfer coefficients, probably resulting from experimental or operator error, led to numerical oscillations, and the corresponding runs had to be omitted from the comparisons. The remaining runs, however, again covered a wide range of data points.

DESIGN CHARTS

Design charts for the different absorber tubes were developed for two sets of operating conditions—those corresponding to water-cooled and air-cooled absorbers (Miller et al. 1992). The design information for each tube includes evaporator load, absorber load, mass absorbed, exit solution concentration and temperature, and degree of subcooling versus tube length. The coolant and inlet solution flow rates are the varying parameters in each plot, while the coolant inlet temperature and absorber pressure are fixed at values representative of water or air cooling.

For the smooth tube, sets for wavy-laminar flows as well as wavy-turbulent flows (roll waves) were obtained. In the case of the three pin-finned tubes, the inlet solution flow rate parameter was varied at slightly higher values for tubes −2 and −3 than for the smooth tube and tube −1 due to a lack of experimental information at low flow rates (0.0025 to 0.0045 kg/s).

The final stage consisted of developing the charts for tubes −4, −5, and −6. For all three tubes, the solution flow rate ranged from 0.0075 to 0.0108 kg/s, which is even higher than the range employed for the latter two pin-finned tubes. Again, this was due to the availability of sufficient experimental data (to calculate the transport coefficients) at these higher flow rates.

The degree of subcooling appears to be a monotonically decreasing function. However, if the subcooling is zero at the solution inlet and zero at the outlet of an infinitely long tube, it must then exhibit a maximum at some intermediate length. This is shown in Figure 11.

A comparison of the performances of the different tubes (as predicted by the model) for the same operating conditions is presented in Table 2. The performance indicator chosen is the evaporator load. Clearly, tube −1 is the best performer, followed by tube −4. The effect of the roll waves is significant in that enhancements of 50% are easily obtained over wavy-laminar flows.

Example of Chart Use

The design charts for absorber tube −1 (1/4-in. pitch, pin-finned) are included here for illustration (Figures 12 through 17).

Absorber Design for Given Head Room—Flow Diagram (Figure 18)

Consider a design load of 10.55 kW at a vapor pressure of 7 mm Hg, with a tube height of 1.0 m. Entering Figure 12 in the abscissas at this height, the load that each tube can handle ranges from 0.6 to 1.3 kW, as bracketed by the curves of constant solution flow rate. Any value between those limits can be obtained by selecting an appropriate combination of coolant and solution flow rates. A low coolant flow results in low parasitic power, whereas a high solution flow may be called upon by the design of the rest of the absorption cycle. Assuming that a combination of low coolant flow (0.082 kg/s) and high solution flow (0.011 kg/s) is desired, the tube can handle approximately 0.88 kW. Thus, 12 tubes are required to handle the given load.

The absorber heat load (Figure 13), the mass absorbed (Figure 14), the solution exit concentration (Figure 15) and temperature (Figure 16), and the subcooling (Figure 17) can

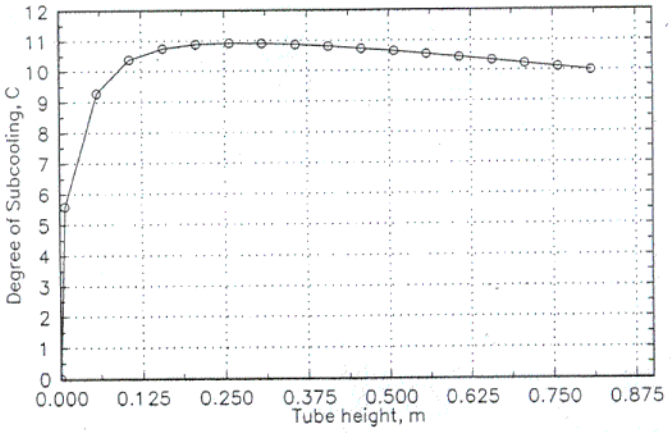

Figure 11 *Illustration of maximum in subcooling function (grooved tube).*

be obtained with a simple reading similar to that used for the evaporator load. Given a coolant flow of 0.082 kg/s and a solution flow of 0.011 kg/s, the 1.0-m-high tube would absorb 0.00035 kg/s of water vapor (Figure 14). The heat load to be removed from the absorber can be looked up in Figure 13 to be 1.0 kW. The concentration and temperature of brine leaving the absorber would be about 58.65 wt% LiBr (Figure 15) and 36°C (Figure 16), respectively, and the solution would leave the absorber about 8.1°C subcooled (Figure 17).

Similar interpretations can be made from the design charts when the prime interest of the designer is minimizing subcooling or the absorber footprint (Miller et al. 1992).

CONCLUSIONS

An analytical model has been developed to estimate vertical-tube absorber performance, within reasonable margins of deviation, using seven different tube surfaces.

The output of the model has been reduced to design charts based on a given set of operating parameters. The complete charts are available in Miller et al. (1992). The charts are performance maps of a falling-film, vertical-tube absorber with different tube surfaces. They allow th determination of absorber size and operating exit condition for a given evaporator load. Thus, if the evaporator load i known and the coolant and solution flow rates are selected the performance map will yield the tube length (Miller et al [1992], Figure 22) and heat load (Miller et al. [1992] Figure 23). The mass absorbed, exit solution concentration temperature, and degree of subcooling can also be read fron the charts (Miller et al. [1992], Figures 24 through 27) fo the obtained absorber length.

Perhaps the most remarkable aspect of this work is th close agreement between Wasden and Dukler's prediction of mass transfer enhancement due to roll waves and thos incorporated in the model. Induced roll waves can enhanc absorption significantly—by a factor of approximately 3. over smooth falling films and approximately 1.5 over wavy laminar films (Yih and Chen 1982).

NOMENCLATURE

A	=	absorption area, m^2
c	=	concentration, kg/m^3
Ga	=	Galelei number (= $L/\bar{\delta}$)
L	=	absorption length
LMCD	=	log-mean concentration difference, kg/m^3
m	=	mass flow rate, kg/s
p	=	wetted perimeter, m
P	=	pressure, mm Hg
Re	=	Reynolds number (= $4m/p\mu$)
Sc	=	Schmidt number
T	=	temperature, °C

Greek Symbols

$\bar{\delta}$	=	average or Nusselt film thickness, m
Δ	=	increase in quantity (by absorption)
κ	=	mass transfer coefficient based on concentra tion differential, m/s
κ_P	=	mass transfer coefficient based on pressu differential, $kg/(m^2 \cdot s \cdot mm\ Hg)$
μ	=	dynamic viscosity, $N \cdot s/m^2$

TABLE 2
Comparison of Evaporator Capacity for 1.5-m-long Tested Tubes
(Coolant Flow = 3 m/s, Solution Mass Flow In = 0.0075 kg/s)

Tube Type	Capacity (kW) @ P = 7 mm Hg, T_{c_i} = 29.4°C	Capacity (kW) @ P = 10 mm Hg, T_{c_i} = 43.3°C
Tube –1	1.67	1.01
Tube –4	1.42	0.87
Tube –2	1.31	0.81
Tube –6	1.12	0.67
Tube –3	0.96	0.59
Tube –5	0.82	0.50
Smooth (Roll Waves)	0.59	0.42
Smooth	0.40	0.29

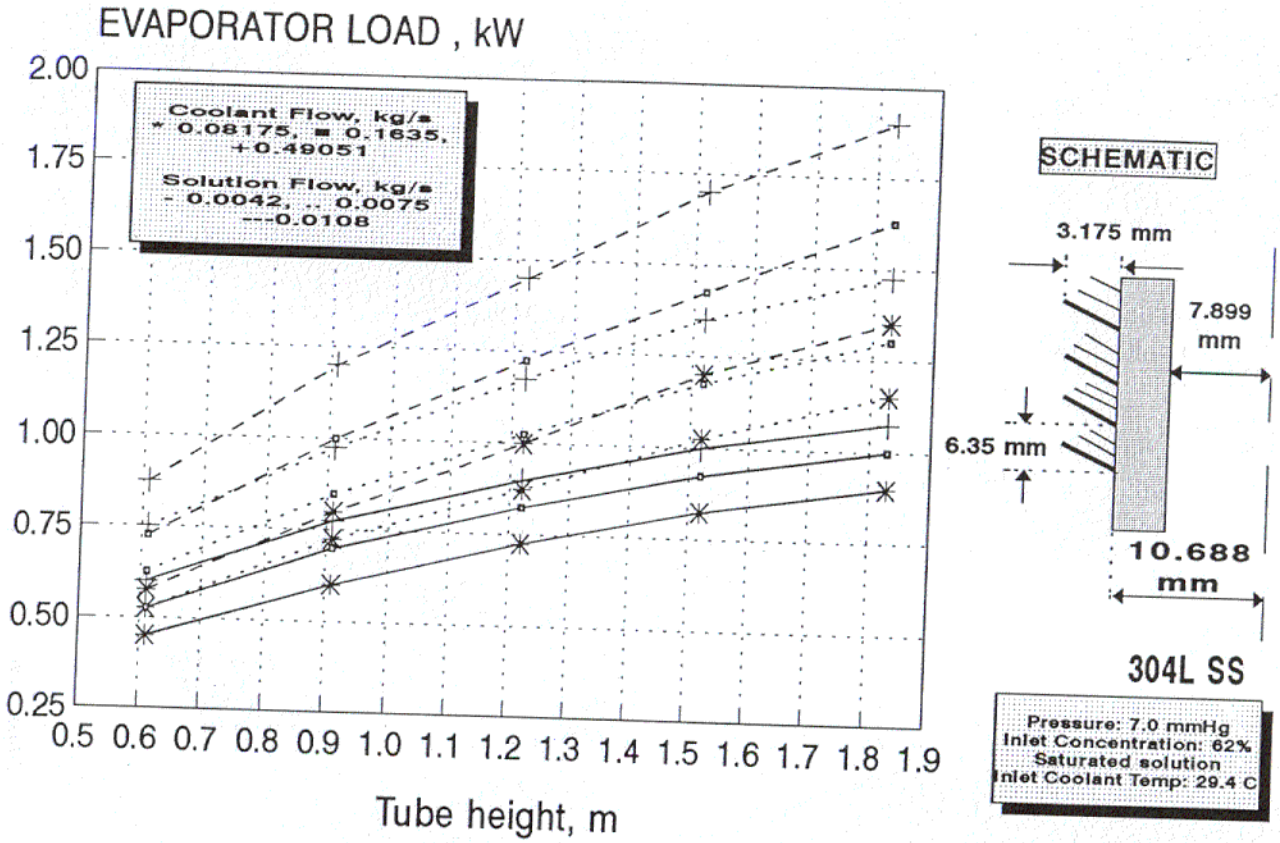

Figure 12 *Design chart for tube –1: evaporator load vs. tube height.*

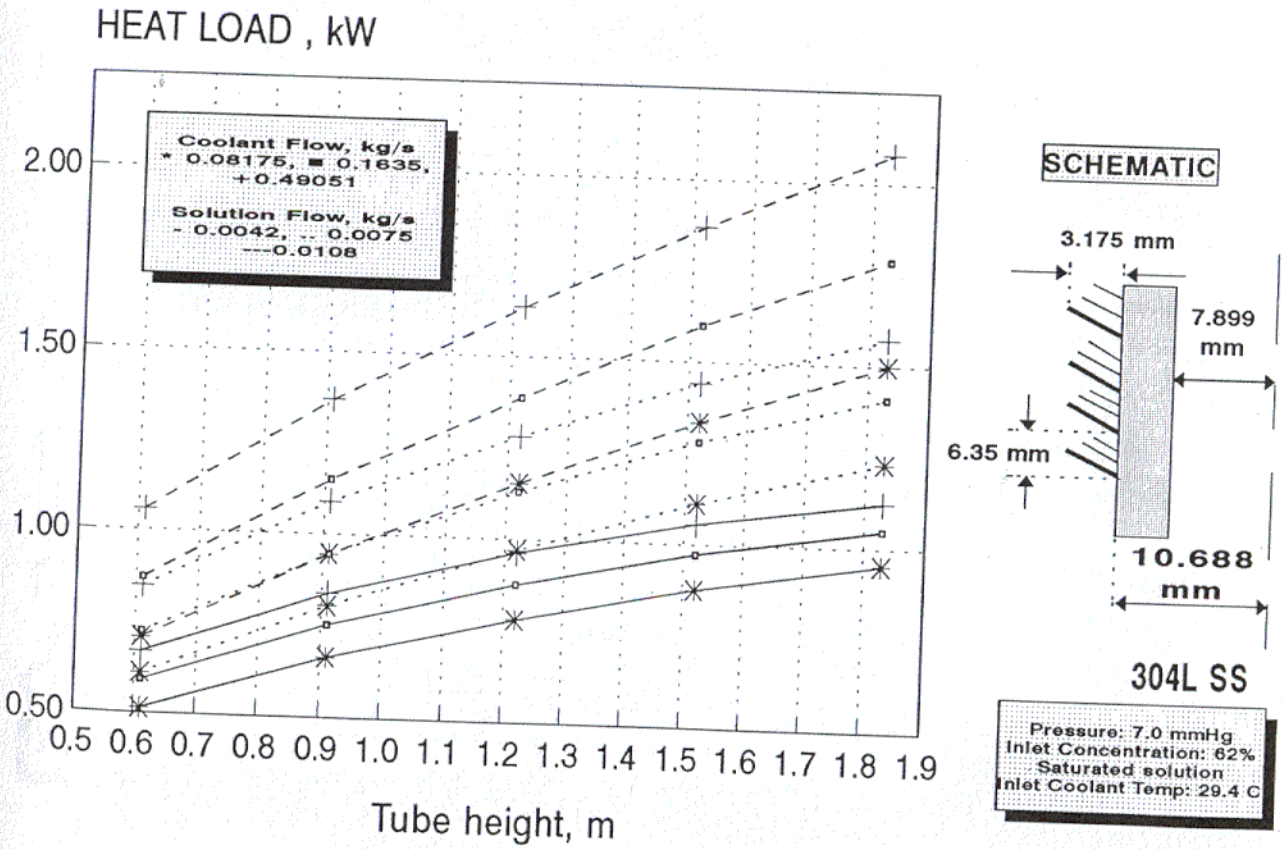

Figure 13 *Design chart for tube –1: heat load vs. tube height.*

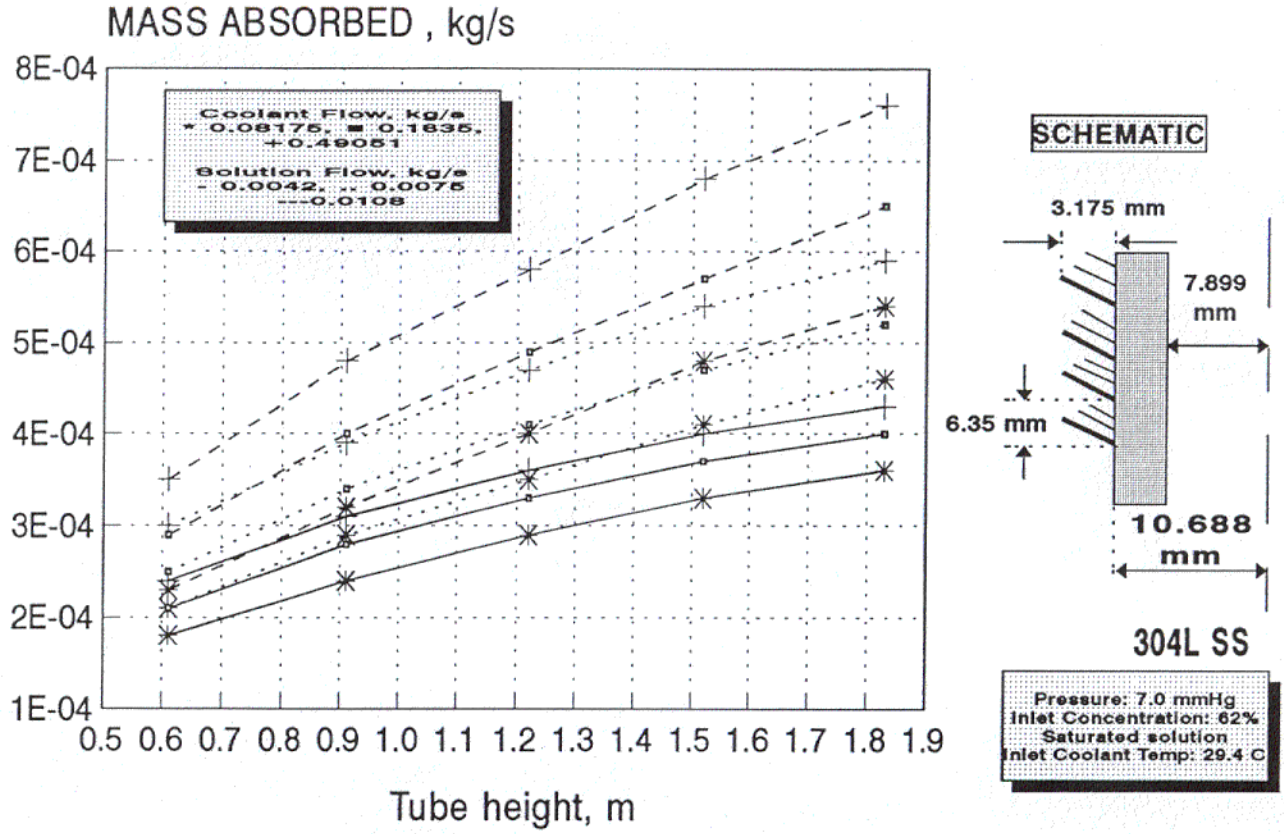

Figure 14 *Design chart for tube −1: mass absorbed vs. tube height.*

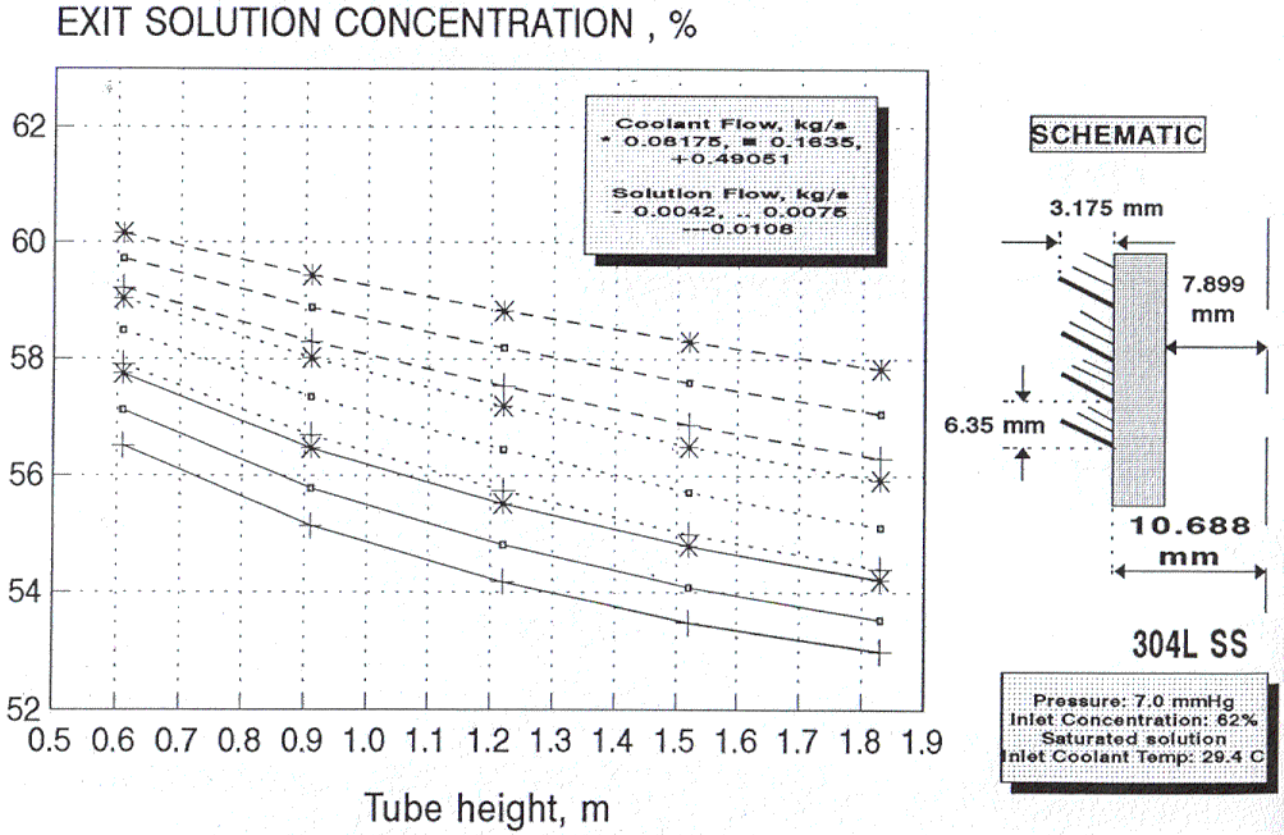

Figure 15 *Design chart for tube −1: exit concentration vs. tube height.*

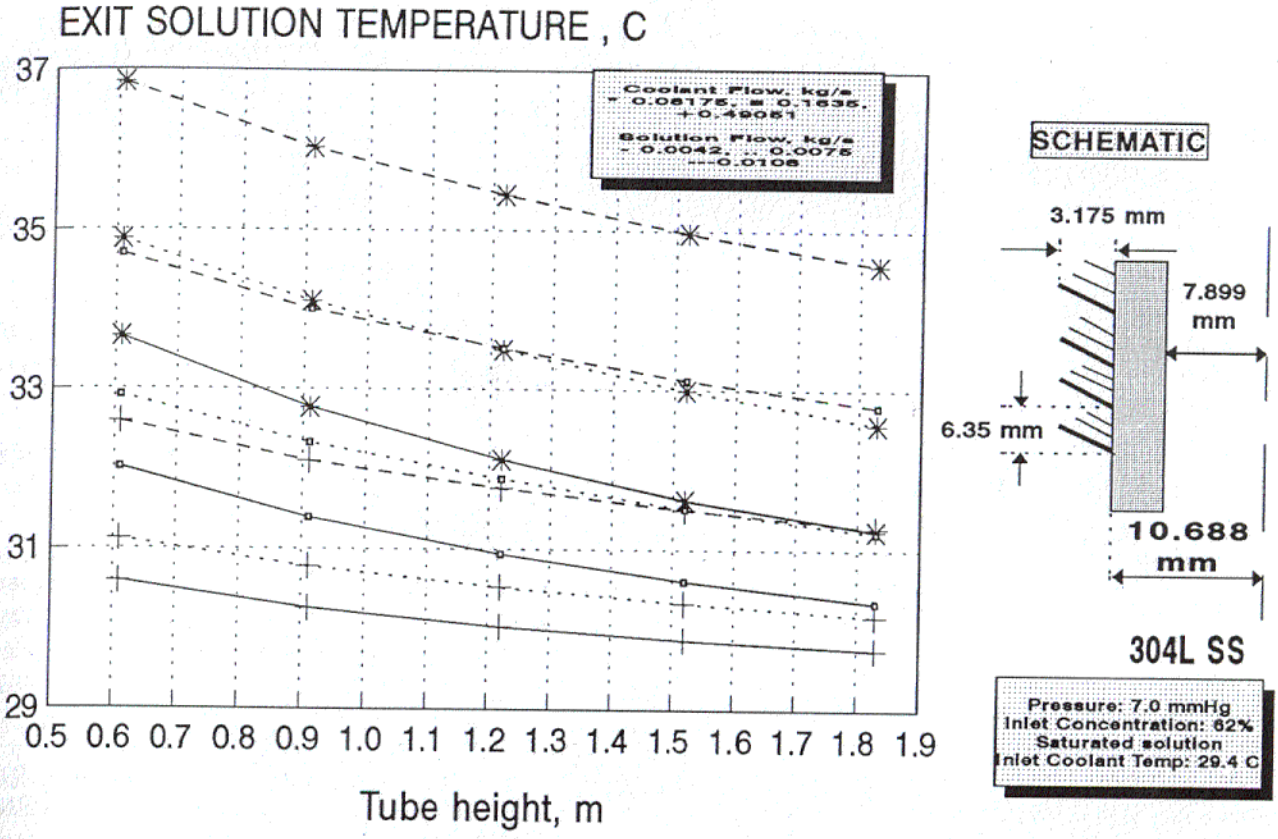

Figure 16 Design chart for tube –1: exit temperature vs. tube height.

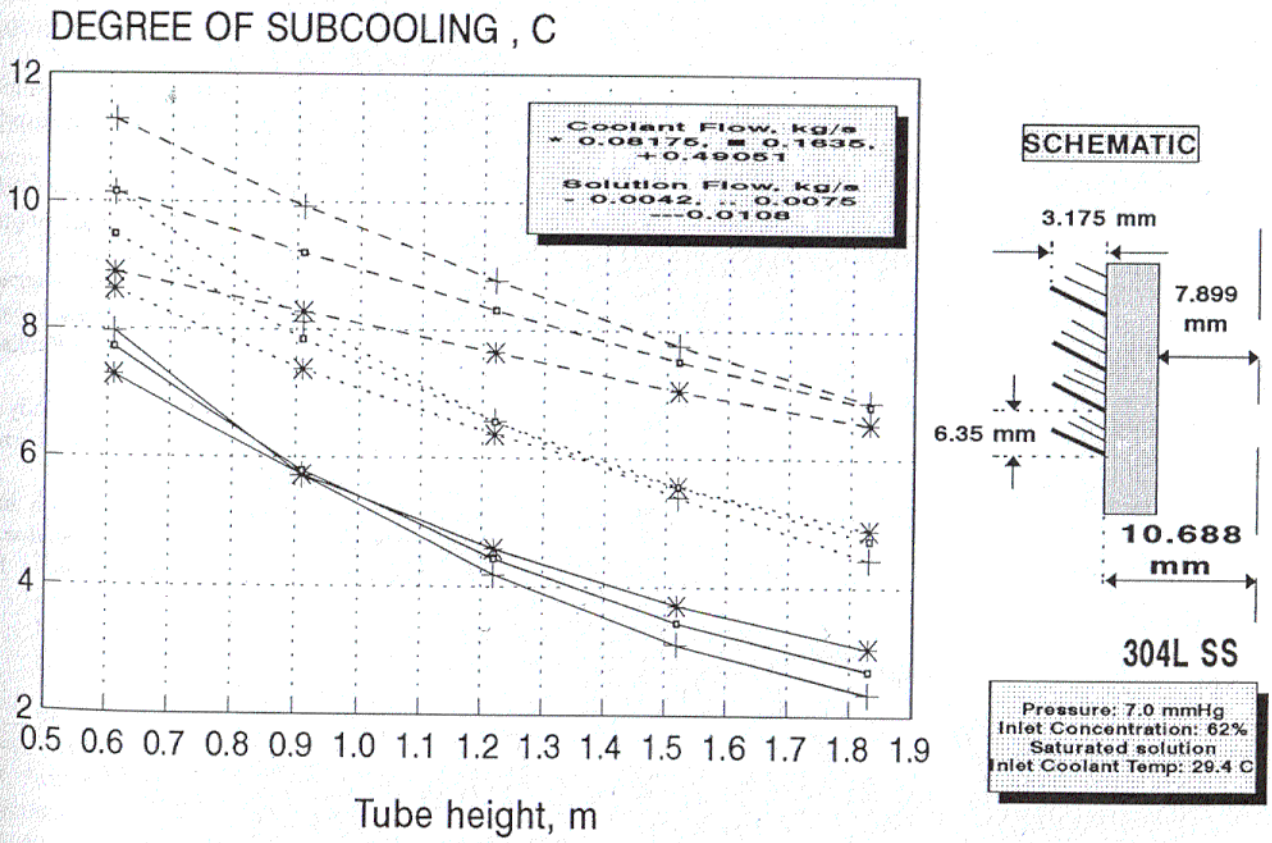

Figure 17 Design chart for tube –1: subcooling vs. tube height.

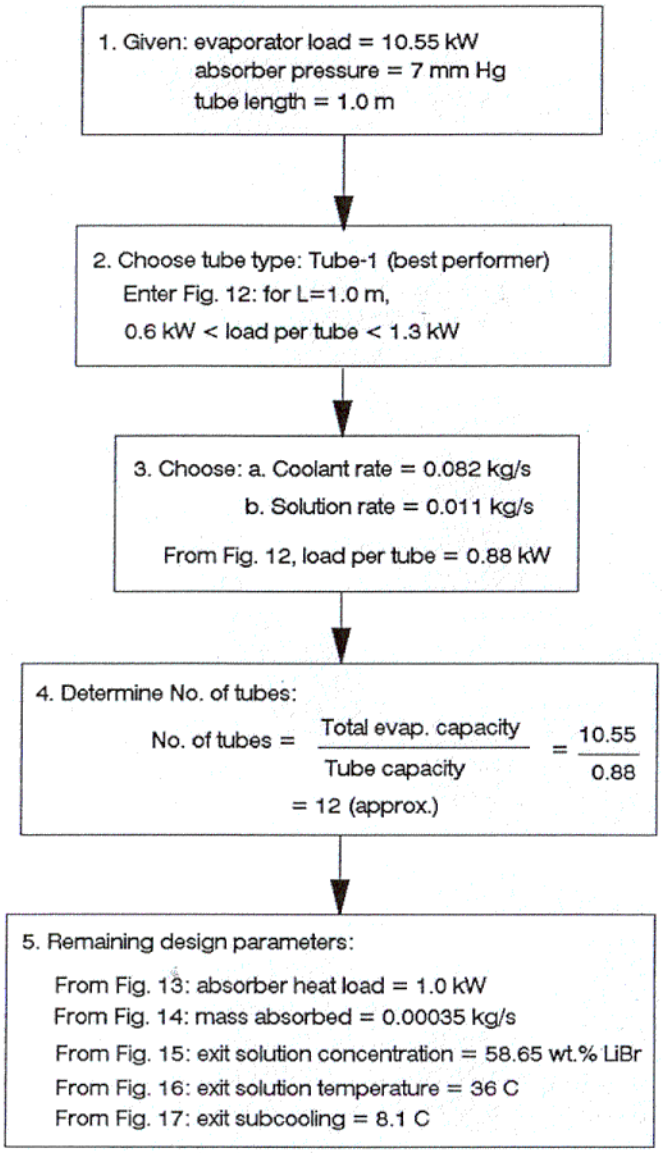

Figure 18 *Absorber design for given head room.*

Subscripts

c	=	coolant
flash	=	"flash" point
i	=	inlet
o	=	outlet
s	=	solution
v	=	vapor

REFERENCES

Brauner, N. 1989. Modeling of wavy flow in turbulent free falling films. *International Journal of Multiphase Flow* 15(4): 505-520.

Jianpin, W., Z. Tianfu, and X. Zhonghuao. 1985. The heat and mass transfer of falling film absorption of aqueous lithium bromide solutions with small Reynolds numbers. *Journal of Zhejiang University* 19(4): 71-81.

Levich, V.G. 1962. Motion and diffusion in thin liquid films. In *Physicochemical Hydrodynamics*, chap. 12. New York: Prentice-Hall, Inc.

Miller, W.A., H. Perez-Blanco, and V. Patnaik. 1992. Advanced surfaces for vertical tube absorbers. ORNL final report to Gas Research Institute (GRI contract no. 5089-243-1844). Oak Ridge, TN: Oak Ridge National Laboratory.

Patnaik, V. 1994. Combined heat and mass transfer in wavy film absorption. Ph.D. thesis. University Park: Pennsylvania State University.

Patnaik, V., H. Perez-Blanco, and W. Ryan. 1993. A simple analytical model for the design of vertical tube absorbers. *ASHRAE Transactions* 99(2).

Ruckenstein, E., and C. Berbente. 1968. Mass transfer to falling liquid films at low Reynolds numbers. *Int. J. Heat Mass Transfer* 11: 743-753.

Seban, R.A. 1978. Transport to falling films. *Sixth International Heat Transfer Conference, Toronto, Canada*, vol. 6, pp. 417-428. Washington, DC: Hemisphere Publishing Corp.

Wasden, F.K., and A.E. Dukler. 1990. A numerical study of mass transfer in free falling wavy films. *AIChE Journal* 36(9): 1379-1390.

Yih, S.-M., and K.-Y. Chen. 1982. Gas absorption into wavy and turbulent falling liquid films in a wetted-wall column. *Chemical Engineering Communications* 17: 123-136.